Dynamic Analysis of Slotless Permanent Magnet Linear Synchronous Motor using the 3-D Space Harmonic Method

Ho-Jin Ahn*, Gyu-Hong Kang and Gyu-Tak Kim****

Abstract - This paper presents the dynamic analysis method for a slotless permanent magnet linear synchronous motor (PMLSM) using the 3-D space harmonic method. Instantaneous emf and thrust are considered by movement of the PM and instantaneous armature current instead of k_E (back-emf constant) and k_F (thrust force constant) for accurate results. The results of magnetic field distribution, back-emf, inductance, and thrust are in agreement with 2-D FEM and experimental results. To confirm the validity of this method, the calculated results are compared to measured ones.

Keywords: dynamic analysis, linear synchronous motor, 3-D space harmonic method

1. Introduction

Recently, the linear motion system that is used in factory automation installations and numerical controlled construction systems has demanded both high speed and high precision to step-up production and improve quality. Rotary motors with transformation systems such as ball-screw fail to satisfy these demands because of friction and backlash [1].

However, the direct drive linear motor contains no friction or backlash, and the slotless permanent magnet linear synchronous motor (PMLSM) avoids detent force, which has a bad influence on the precision control. Moreover, the slotless PMLSM is not only highly precise, but also performs at high speed using the high energy density permanent magnet. Therefore, the slotless PMLSM is an optimal driving source in the linear motion system. Thus, this paper deals with the characteristic analysis for the slotless PMLSM.

To calculate the airgap field distribution of the slotless PMLSM, the space harmonic method is more reasonable than the finite element method (FEM) because of its simple structure and large magnetic airgap [1-2].

Therefore, this paper presents the static and dynamic analysis method for the slotless PMLSM using the space harmonic method and proposes the 3-D airgap field distribution considering end-coil.

Generally, linear motors are driven under the transient state because of their short structure. Thus, starting and braking characteristics must be considered when designing linear motors. This paper analyzes the starting characteristic of the slotless PMLSM under open-loop control using 3-D airgap field distributions. In this paper, instantaneous emf and thrust are considered from the instantaneous PM and armature field instead of k_E (back-emf constant) and k_F (thrust force constant) because each phase current lack equilibrium and sine wave in the starting and braking state.

2. Analysis model

Fig. 1 shows the side view of a single side moving magnet slotless PMLSM. The main dimensions and specifications are listed in Table 1.

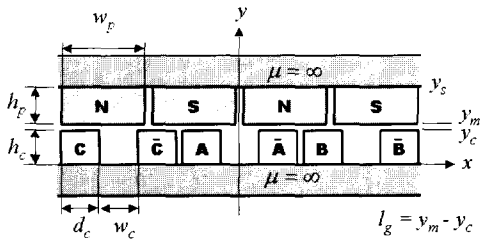

Fig. 1 Side view of analysis model

Table 1 Specification of analysis model

item	symbol	value [unit]
pole pair	p	6 [EA]
residual induction	B_r	1.2 [T]
PM size	h_p x w_p x l_p	12 x 26 x 73.5 [mm]
pole pitch	τ_p	28.5 [mm]
turn number/coil	N	650 [EA]
coil area	h_c x w_c	11 x 12 [mm]
coil distance	d_c	12 [mm]
phase current (max)	I	2.66 [A]
airgap length	l_g	2 [mm]

* Engineer in the Mi-Rae Industrial Research Institute Co. Ltd., Osan-ri, Dontan-Myun, Hwasung, Korea (hojin2@hotmail.com)
** Department of Electrical Engineering, Changwon National University, Sarimdong, Changwon, Korea (kgh1004@cosmos.changwon.ac.kr, gtkim@sarim.changwon.ac.kr)
Received September 16, 2002 ; Accepted November 12, 2002

3. Three-dimensional airgap field distribution

The space harmonic method is much faster than the FEM, and in unsaturated and simple models, the results are in good agreement with the FEM. Thus, the space harmonic method is widely used in early designs or characteristic analysis according to changes in the design parameters.

For the expediency calculation, this paper presents the following assumptions.

① The analysis region is unlimited through the x and z directions.

② The magnetization of the PM and the current are uniform to the y-axis direction and have a very far cycle periodic distribution along the z-axis.

③ The magnetic permeability of the core is infinite.

3.1 Magnetic field of PM

Generally, the magnetic vector potential **A** is used as a field variable in the magnetic field calculation, but to use the magnetic vector potential, the magnet distribution must be transformed to the equivalent magnetizing current and must calculate 3 values of the vector potential, x, y, and z-components of the vector potential. This operation is very troublesome. Thus, this paper uses the magnetic scalar potential φ.

Equations (1) and (2) are the governing equations in the air (region I) and magnet (region II) regions, respectively.

$$\nabla^2 \varphi_{Air}^{pm} = 0 \tag{1}$$

$$\nabla^2 \varphi_{Magnet}^{pm} = \frac{\nabla \cdot \dot{M}_y}{\mu_r} = 0 \tag{2}$$

Here M_y is the magnetization vector of the PM, and Fig. 2 shows this distribution. This paper assumes that magnetization is uniform to the y-axis direction, so the right term would be 0.

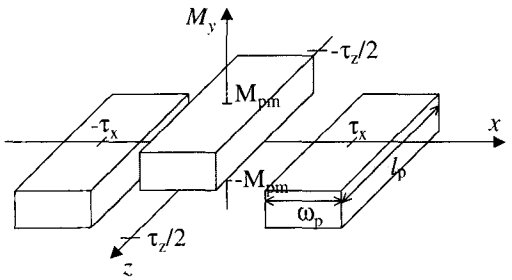

Fig. 2 The PM's magnetization distribution

This magnetization distribution is represented as Eq. (3) using the Fourier series.

$$M_y = \sum_{m=1}^{\infty}\sum_{n=1}^{\infty} M_{mn}\cos(mk_x x)\cos(nk_z z) \tag{3}$$

$$M_{mn} = \frac{16M_{pm}}{mn\pi^2}\sin(m\alpha_x\frac{\pi}{2})\sin(n\alpha_z\frac{\pi}{2}) \quad (m,n = 1,3,5,\ldots) \tag{4}$$

Here the coefficients k_x, k_z, α_x and α_z are represented as shown in Eq. (5). α_x and α_z are the pole ratios to the x and z directions, respectively; and k_{mn} has the relationship shown in Eq. (6).

$$k_x = \frac{\pi}{\tau_x},\ k_z = \frac{\pi}{\tau_z},\ \alpha_x = \frac{w_p}{\tau_x},\ \alpha_z = \frac{l_p}{\tau_z} \tag{5}$$

$$k_{mn}^2 = m^2k_x^2 + n^2k_z^2 \tag{6}$$

From the general solution of Eqs. (1) and (2) and the boundary condition, the airgap flux density can be written in the following forms.

$$B_{x\,Air}^{pm} = -\sum_{m=1,3,\ldots}^{\infty}\sum_{n=1,3,\ldots}^{\infty}\frac{mk_x}{k_{mn}}\beta_m\sinh(k_{mn}y)\cdot\sin(mk_x x)\cos(nk_z z) \tag{7}$$

$$B_{y\,Air}^{pm} = +\sum_{m=1,3,\ldots}^{\infty}\sum_{n=1,3,\ldots}^{\infty}\beta_m\cosh(k_{mn}y)\cos(mk_x x)\cdot\cos(nk_z z) \tag{8}$$

$$B_{z\,Air}^{pm} = -\sum_{m=1,3,\ldots}^{\infty}\sum_{n=1,3,\ldots}^{\infty}\frac{nk_z}{k_{mn}}\beta_m\sinh(k_{mn}y)\cdot\cos(mk_x x)\sin(nk_z z) \tag{9}$$

Here β_m is given by

$$\beta_m = \frac{\mu_0 M_{mn}\sinh(k_{mn}(y_m - y_s))}{\xi_m}$$
$$\xi_m = \mu_r\cosh(k_{mn}y_m)\sinh(k_{mn}(y_m - y_s)) - \cosh(k_{mn}(y_m - y_s))\sinh(k_{mn}y_m) \tag{10}$$

3.2 Magnetic field of armature current

The 3-D field distribution of the current calculation is more difficult than the field of the PM because of the half-circle shape of the end-coil. Thus, in this paper, the shape is assumed to be rectangular as in Fig. 3. The areas of the two end-coil shape types are the same. The magnetization

of the armature current that has a rectangular end-coil can be expressed as in Fig. 4.

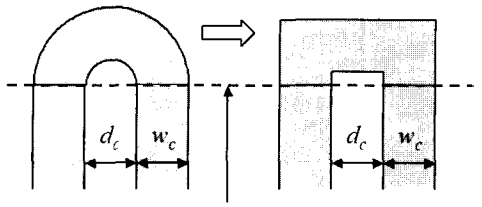

Fig. 3 Equivalence of end-coil area

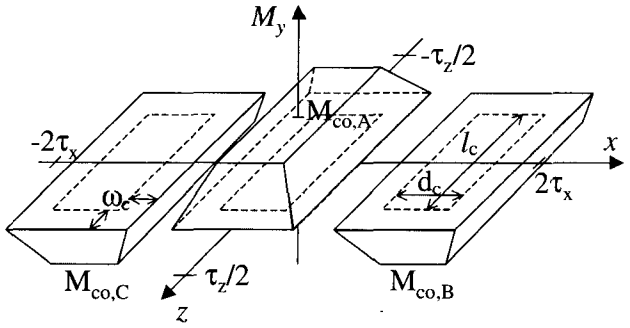

Fig. 4 Armature current magnetization distribution

The magnetization distribution of the armature current is similar to the magnetization of the PM, so the distribution can be represented as Eq. (3), and Fourier's coefficient M_{mn} can be written in the following form.

$$M_{mn} = \frac{32M_{co}}{m^2n^2\pi^2}\frac{1}{k_x k_z w_c^2}\sin(mk_x\frac{d_c+w_c}{2})\sin(mk_x\frac{w_c}{2}) \cdot\sin(nk_z\frac{l_c+w_c}{2})\sin(nk_z\frac{w_c}{2}) \quad (m=1,2,3,\ldots\ n=1,3,5,\ldots) \tag{11}$$

Using the same process of flux density calculation of the PM, the airgap flux density distribution can be expressed as Eq. (13).

$$B_{x\,Air}^{co} = +\sum_{p=1}^{3}\sum_{m=1}^{\infty}\sum_{n=1,3,\ldots}^{\infty}\frac{mk_x}{k_{mn}}\beta_{co}\cos(\omega t+\frac{2\pi}{3}(p-1)) \cdot\sinh(k_{mn}(y-y_s))\cdot\sin[m(k_x x-\frac{2\pi}{3}(p-1))] \cdot\cos(nk_z z) \tag{12}$$

$$B_{y\,Air}^{co} = -\sum_{p=1}^{3}\sum_{m=1}^{\infty}\sum_{n=1,3,\ldots}^{\infty}\beta_{co}\cos(\omega t+\frac{2\pi}{3}(p-1)) \cdot\cosh(k_{mn}(y-y_s))\cdot\cos[m(k_x x-\frac{2\pi}{3}(p-1))] \cdot\cos(nk_z z) \tag{13}$$

$$B_{z\,Air}^{co} = +\sum_{p=1}^{3}\sum_{m=1}^{\infty}\sum_{n=1,3,\ldots}^{\infty}\frac{mk_x}{k_{mn}}\beta_{co}\cos(\omega t+\frac{2\pi}{3}(p-1)) \cdot\sinh(k_{mn}(y-y_s))\cdot\cos[m(k_x x-\frac{2\pi}{3}(p-1))] \cdot\sin(nk_z z) \tag{14}$$

Here β_{co} is given by

$$\beta_{co} = \frac{\mu_0 M_{mn}\sinh(k_{mn}y_c)}{\xi_c}$$
$$\xi_c = \cosh(k_{mn}y_c)\sinh(k_{mn}(y_c-y_s)) - \cosh(k_{mn}(y_c-y_s))\sinh(k_{mn}y_c) \tag{15}$$

Fig. 5 shows the PM's and current's magnetic field distribution using Eqs. (7) ~ (9) and Eqs. (12) ~ (14), respectively.

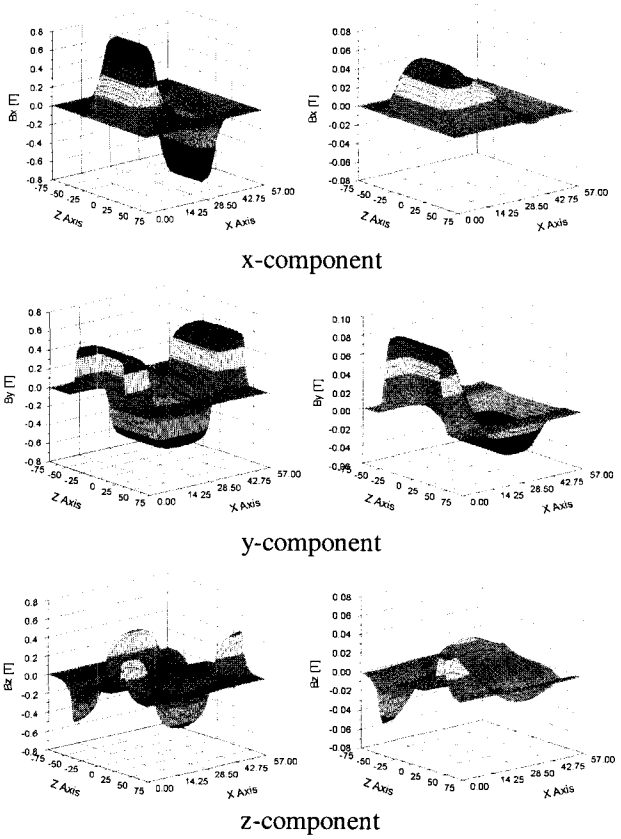

(a) PM airgap field (b) Current airgap field

Fig. 5 Magnetic field distributions at the airgap

3.3 Back-emf and inductance

Back-EMF is computed by changing a flux linkage in the coils and by integrating the y-component among the flux densities of the PM as shown in Fig. 6 and Eq. (16).

$$e_a = N\left[B^{pm}{}_y\Big|_{x=x_1} - B^{pm}{}_y\Big|_{x=x_2}\right]_{y=y_1/2} \cdot l_z \cdot v \qquad (16)$$

Here, N is the number of turns, l_z is the length of the z-axis, v is the velocity, and $B^{pm}{}_y\big|_{x=x_1}$ is the flux density in the coil at $x=x_1$.

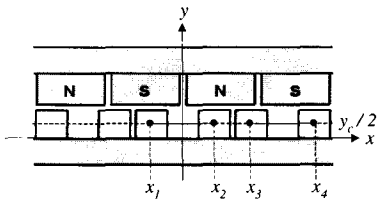

Fig. 6 Integral path for back-EMF and inductance calculation

Fig. 7 shows that the result of the 2-D space harmonic method is in agreement with the corresponding 2-D FEM, and a 5% error exists between the 2-D and 3-D space harmonic methods.

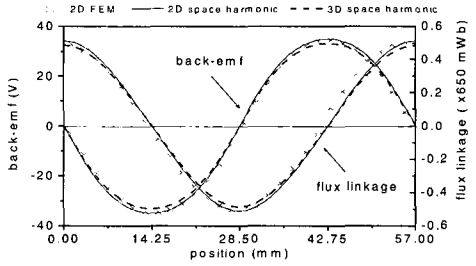

Fig. 7 Back-emf and flux linkage

Inductance is calculated using Eqs. (17) and (18).

$$L = \frac{N\Phi}{I} = \left.\frac{Nl_z\int_{x_1}^{x_2} B^{co}{}_{yII}\,dx}{I}\right|_{exiting\ one\ phase} \qquad (17)$$

$$M = \frac{N\Phi}{I} = \left.\frac{Nl_z\int_{x_3}^{x_4} B^{co}{}_{yII}\,dx}{I}\right|_{exiting\ one\ phase} \qquad (18)$$

Table 2 shows each method's calculated inductance. There are some errors, but in the slotless PMLSM, winding resistance is much larger than reactance, so accuracy of inductance is unimportant.

Table 2 Comparison of inductance (R=18.2Ω)

	2-D FEM	2-D SHM	3-D SHM	measured
Self [mH]	30.86	34.25	30.03	29.38
Mutual [mH]	9.08	9.07	8.46	-

(Note : Space harmonic method is abbreviated as SHM.)

Thrust and normal force can be calculated using the Maxwell stress tensor method. Fig. 8 shows that thrust of the 2-D space harmonic method is in agreement with the 2-D FEM and that the 3-D space harmonic is in agreement with the experimental result.

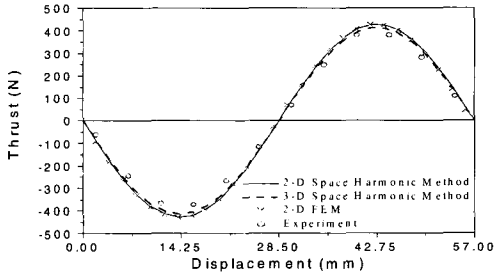

Fig. 8 Thrust according to displacement

4. Starting characteristic analysis

Generally, in linear motors, the starting characteristic is more important than the static characteristic because liner motors are driven under the transient state by reason of their short stroke. The starting characteristic can be analyzed by combining the voltage equation with the dynamic equation. In general, thrust and back-emf are calculated by the thrust force constant k_F and emf constant k_E indirectly. However, with the transient state as the starting region, the use of thrust and force constant cause error because each phase current lacks equilibrium and sinewave in the transient state. Therefore, this paper presents instantaneous thrust and emf instead of k_F and k_E. Instantaneous emf and thrust can be calculated by moving the x-coordinate of PM. Fig. 9 shows the analysis process of proposed method. Eq. (19) is a three-phase voltage equation.

$$\begin{bmatrix} V_a \\ V_b \\ V_c \end{bmatrix} = R\begin{bmatrix} i_a \\ i_b \\ i_c \end{bmatrix} + \frac{d}{dt}\begin{bmatrix} L & M & M \\ M & L & M \\ M & M & L \end{bmatrix}\begin{bmatrix} i_a \\ i_b \\ i_c \end{bmatrix} + \begin{bmatrix} e_a \\ e_b \\ e_c \end{bmatrix} \qquad (19)$$

This paper analyzed the starting characteristic of the slotless PMLSM under open-loop control. Parameters vary, but *V/f* ratio and initial load angle are selected out of many control parameters in this paper. Table 3 shows the parameters for the starting characteristic analysis of this paper.

Table 3 Parameters for the starting characteristic analysis

item	value	item	value
voltage	0 ~ 100 [V]	rated speed	2 [m/s]
frequency	0 ~ 35 [Hz]	synchronous frequency	35.1 [Hz]
rated voltage	100 [V_p]	mass of mover	30 [kg]
raged current	2.66 [A_p]	acceleration	1.0 G

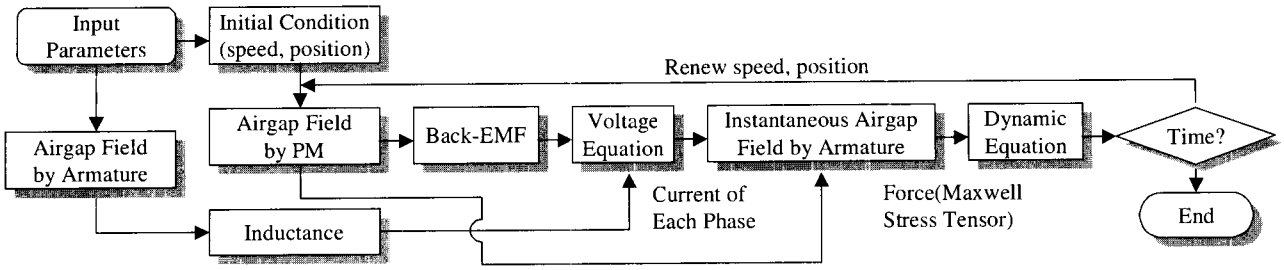

Fig. 9 Process of dynamic analysis

4.1 Starting characteristic according to V/f ratio

Fig. 10 shows the speed curve at the starting region. In Fig 10(a), the starting characteristic performs poorly with a sudden change of load angle because the starting current is too high for the rated current under full voltage. Fig. 11 shows that the power factor is near 1 because the resistance is larger than the reactance in the slotless PMLSM.

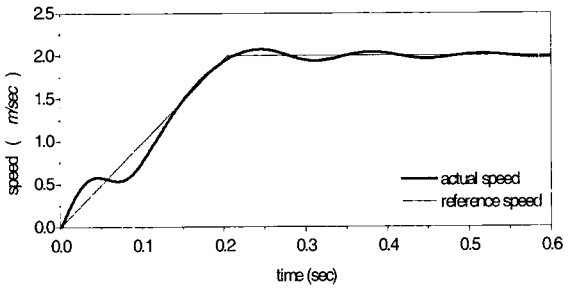

(a) V=100

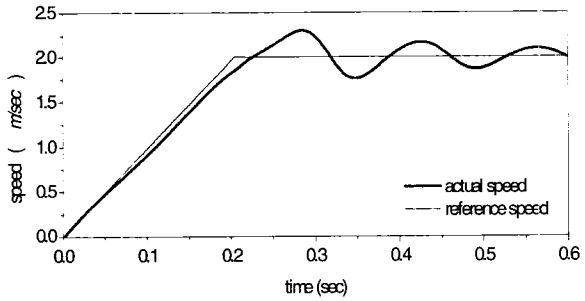

(b) V=1.5f + 47

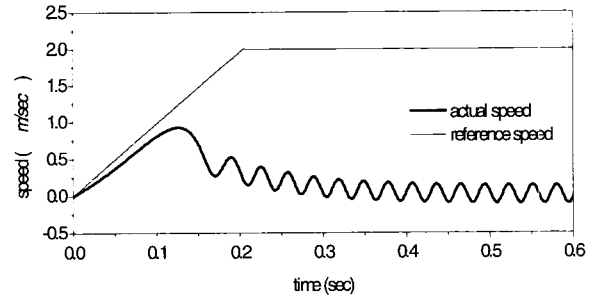

(c) V=2.0f + 40

Fig. 10 Starting characteristics according to V/f ratio(initial load angle = 90 deg., no load)

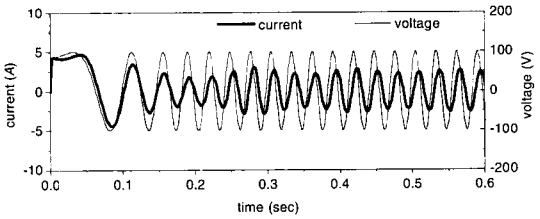

Fig. 11 A-phase current and voltage (V=100)

4.2 Starting characteristic according initial load angle

Fig. 12 shows the starting characteristic according to the initial load angle under no load and V=1.0f + 65. Although the initial load angle is 90 degrees, failure to start is possible due to the rapid change of load angle.

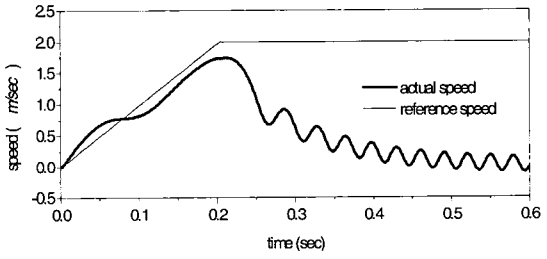

(a) initial load angle = 90 degrees

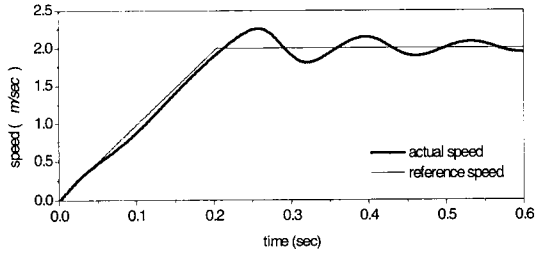

(b) initial load angle = 45 degrees

Fig. 12 Starting characteristic according to initial load angle

The results show that the V/f ratio should be changed according to the initial load angle or the other condition. However, under open-loop control, finding the optimal V/f ratio is very difficult. For this reason, this paper presents no optimal V/f ratio under the variable drive condition. PMLSMs are driven under closed-loop control in general and their starting characteristic is predicted not only by the

specificity of the motor, but also by the specificity of the controller under closed-loop control. Therefore, control method and the specificity of the controller should be considered for dynamic simulation of slotless PMLSMs.

5. Conclusions

This paper presents the starting characteristic analysis method of the slotless PMLSM under open-loop control using the 3-D space harmonic method. The results of magnetic field distribution, back-emf, inductances and thrust agree with 2-D FEM and experimental results. In this paper, instantaneous back-emf and thrust are considered instead of k_E and k_F because each phase current lacks equilibrium and sinewave in the starting region.

Acknowledgments

This work was supported by the Korea Science and Engineering Foundation (KOSEF) through the Machine Tool Research Center at Changwon National University.

References

[1] I. Boldea and S. A. Nasar, *Linear Motion Electromagnetic Systems*, John Wiley and Sons, 1985.

[2] Z. Q. Zhu and D. Howe, "Instantaneous Magnetic Field Distribution in Permanent Magnet Brushless DC motors", IEEE Trans. on MAGNETICS, Vol. 29, No. 1, pp. 152-158, 1993.

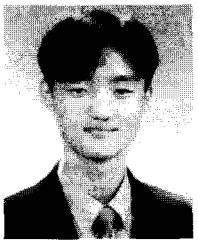

Ho-Jin Ahn
He was born in Korea in 1977. He received the B.S. and M.S. degrees in Electrical Engineering from Changwon National University in 2000 and 2002, respectively. He is currently a research engineer for Mi-Rae Industrial Co. Ltd.
Tel: +82-31-3791-800
Fax: +82-31-3791-801

Gyu-Hong Kang
He was born in Korea in 1967. He received the B.S. and M.S. degrees in Electrical Engineering from Changwon National University in 1992 and 1994, respectively. From 1994 to 1998, he was a research engineer for LG. Elec. Co. Ltd. He received the Ph.D. degree in Electric Engineering from Changwon National University in 2001. Since 2001, he has been a lecturer in the Department of Mecha-tronics at Changwon National University, Changwon, Korea.
Tel: +82-55-279-8044, Fax: +82-55-263-9956

Gyu-Tak Kim
He was born in Korea in 1961. He received the B.Eng., M.Eng. and Ph.D. degrees from Han-Yang University, Seoul, Korea. Since 1991, he has been Lecturer in the Department of Electical Engineering at Changwon National University, Changwon, Korea. Between 1996 and 2001, he was a visiting researcher at Waseda University, Tokyo, Japan. His interests include numerical analysis of electrical machines, and energy conversion theory.
Tel: +82-55-279-7515, Fax: +82-55-263-9956